A seven-coordinate Mn(ii) complex with a pyridine-based 15-membered macrocyclic ligand containing one acetate pendant arm: structure, stability and relaxation properties

Marie Pražáková, Daouda Ndiaye, Éva Tóth, Bohuslav Drahoš

Dalton Transactions

ROYAL SOCIETY OF CHEMISTRY

PAPER

View Article Online
View Journal | View Issue

Check for updates

Cite this: *Dalton Trans.*, 2023, **52**, 7936

A seven-coordinate Mn(II) complex with a pyridine-based 15-membered macrocyclic ligand containing one acetate pendant arm: structure, stability and relaxation properties†

Marie Pražáková, [a] Daouda Ndiaye,[b] Éva Tóth *[b] and Bohuslav Drahoš *[a]

A new 15-membered pyridine-based macrocyclic ligand containing one acetate pendant arm (*N*-carboxymethyl-3,12,18-triaza-6,9-dioxabicyclo[12.3.1]octadeca-1(18),14,16-triene, **L1**) was synthesized and its Mn(II) complex **MnL1** was investigated in the context of MRI contrast agent development. The X-ray molecular structure of **MnL1** confirmed a coordination number of seven with an axially compressed pentagonal bipyramidal geometry and one coordination site available for an inner-sphere water molecule. The protonation constants of **L1** and the stability constants of Mn(II), Zn(II), Cu(II) and Ca(II) complexes were determined by potentiometry, and revealed higher thermodynamic stabilities in comparison with complexes of 15-pyN_3O_2, the parent macrocycle without an acetate pendant arm. The **MnL1** complex is fully formed at physiological pH 7.4, but it shows fast dissociation kinetics, as followed by relaxometry in the presence of an excess of Zn(II). The short dissociation half-life estimated for physiological pH (*ca.* 3 minutes) is related to fast spontaneous dissociation of the non-protonated complex. At lower pH values, the proton-assisted dissociation pathway becomes important, while the Zn(II) concentration has no effect on the dissociation rate. ^{17}O NMR and ^{1}H NMRD data indicated the presence of one inner-sphere water molecule with a rather slow exchange (k_{ex}^{298} = 4.5 × 10^6 s^{-1}) and provided information about other microscopic parameters governing relaxation. The relaxivity (r_1 = 2.45 mM^{-1} s^{-1} at 20 MHz, 25 °C) corresponds to typical values for monohydrated Mn(II) chelates. Overall, the acetate pendant arm in **L1** has a beneficial effect with respect to 15-pyN_3O_2 in increasing the thermodynamic stability and kinetic inertness of its Mn(II) complex, but leads to a reduced number of inner-sphere water molecules and thus lower relaxivity.

Received 7th March 2023,
Accepted 9th May 2023

DOI: 10.1039/d3dt00701d

rsc.li/dalton

Introduction

Magnetic Resonance Imaging (MRI) is one of the most powerful non-invasive diagnostic techniques in medicine for the visualization of soft tissues without radiation load. Since the description of the theory and the first MR images in 1971 reported by Paul C. Lauterbur and later by P. Mansfield,[1,2] and the first animal tumor imaging in 1976,[3] huge progress has been made in MRI physics, instrumentation, and the chemistry of contrast agents (CAs) that are injected into patients to improve image quality.

Due to the low sensitivity and insufficient image contrast, the use of CAs is often required in MRI. These paramagnetic substances reduce the longitudinal (T_1) and transverse (T_2) relaxation times of water protons,[4] and enhance image contrast between different tissues. The majority of CAs are based on paramagnetic metal ions, which are chelated in stable complexes to prevent *in vivo* toxicity of the free metal. Paramagnetic metal complexes affect mainly the longitudinal relaxation of tissue water protons, leading to an increased signal intensity (positive contrast) on T_1-weighted MR images (T_1-CAs).

For over 35 years, Gd(III) chelates have been used in millions of human examinations and are considered as safe diagnostic drugs. However, recent findings associated Nephrogenic Systemic Fibrosis (NSF), a potentially lethal disease, with the use of Gd(III) agents in kidney impaired patients.[5,6] Furthermore, gadolinium deposits, although without toxic effects, have been identified after Gd-enhanced MRI in the

[a]*Department of Inorganic Chemistry, Faculty of Science, Palacký University Olomouc, 17. listopadu 12, 771 46 Olomouc, Czech Republic.*
E-mail: bohuslav.drahos@upol.cz; Fax: +420 585 634 954; Tel: +420 585 634 429
[b]*Centre de Biophysique Moléculaire, CNRS-UPR 4301, Université d'Orléans, rue Charles Sadron, 45071 Orléans, France. E-mail: eva.jakabtoth@cnrs-orleans.fr; Fax: +33-23863151*

†Electronic supplementary information (ESI) available: 2D NMR spectra, more X-ray analysis details, dissociation kinetics results, potentiometric titration curves and equations for analysis of ^{17}O NMR and ^{1}H NMRD data. CCDC 2244643. For ESI and crystallographic data in CIF or other electronic format see DOI: https://doi.org/10.1039/d3dt00701d

bones or the brain of patients even without renal problems.[7,8] As a consequence, the clinical use of Gd(III) chelates formed with linear chelators has been stopped or restricted by control authorities both in Europe and the US. In parallel, the development of more biocompatible alternatives to Gd(III)-based agents has become an active area of research. In this context, complexes of paramagnetic transition metal ions, in particular Mn(II), have been widely investigated, and one Mn(II) chelate is currently in clinical trials.[9] Indeed, the d^5 high spin configuration, slow electron spin relaxation and fast water exchange make Mn(II) the most promising substitute for Gd(III).[10–12]

In general, six- or seven-coordinate Mn(II) chelates, formed with penta- or hexadentate ligands and containing at least one hydration water, can be considered as good contrast agent candidates. The presence of inner sphere water is indispensable in order to achieve good relaxivities. Relaxivity, r_1, is the paramagnetic enhancement of the longitudinal water proton relaxation rates in the presence of 1 mM concentration of the paramagnetic probe, and it directly translates to MRI efficacy. High thermodynamic and redox stability, as well as kinetic inertness, are also required properties for Mn(II) complexes, due to the potential risk associated with the administration of the Mn(II) ion in high concentrations.[13] A major issue could be brain accumulation of Mn(II) causing a neurological disorder ("manganism") with symptoms similar to Parkinson's disease.[14] Macrocyclic ligands are typically better candidates for Mn(II) complexation than non-cyclic analogues, since they allow higher thermodynamic stability and kinetic inertness.[10,15,16] The thermodynamic stability of Mn(II) complexes is lower in comparison with other transition metal analogues due to the lack of ligand-field stabilization energy for the high spin d^5 configuration, as well as in comparison with Gd(III) chelates due to the smaller charge of Mn^{2+}. Few Mn(II) chelates were found to be inert to Zn^{2+} or Cu^{2+} transmetalation,[17,18] although recent examples of Mn(II) bispidine complexes evidence that extraordinary inertness might be possible with highly preorganized and rigid ligand structures.[19]

Pyridine-based macrocycles have been extensively explored for Mn(II) complexation. In 2010, we reported 15-pyN_5 and 15-pyN_3O_2,[20] the pyridine containing analogues of previously studied ligands 15-aneN_5 and 15-aneN_3O_2 (Scheme 1).[21–24] We confirmed that the incorporation of a pyridine moiety into the polyaza macrocycle scaffold leads to higher thermodynamic stability and kinetic inertness. This was particularly true for 15-pyN_5, where the two additional nitrogen atoms result in higher basicity and higher thermodynamic stability for Mn(II), while thanks to the two inner sphere water molecules (q = 2 for an overall coordination number of 7), high relaxivity is retained. More recently, the 15-pyN_3O_2Ph derivative containing

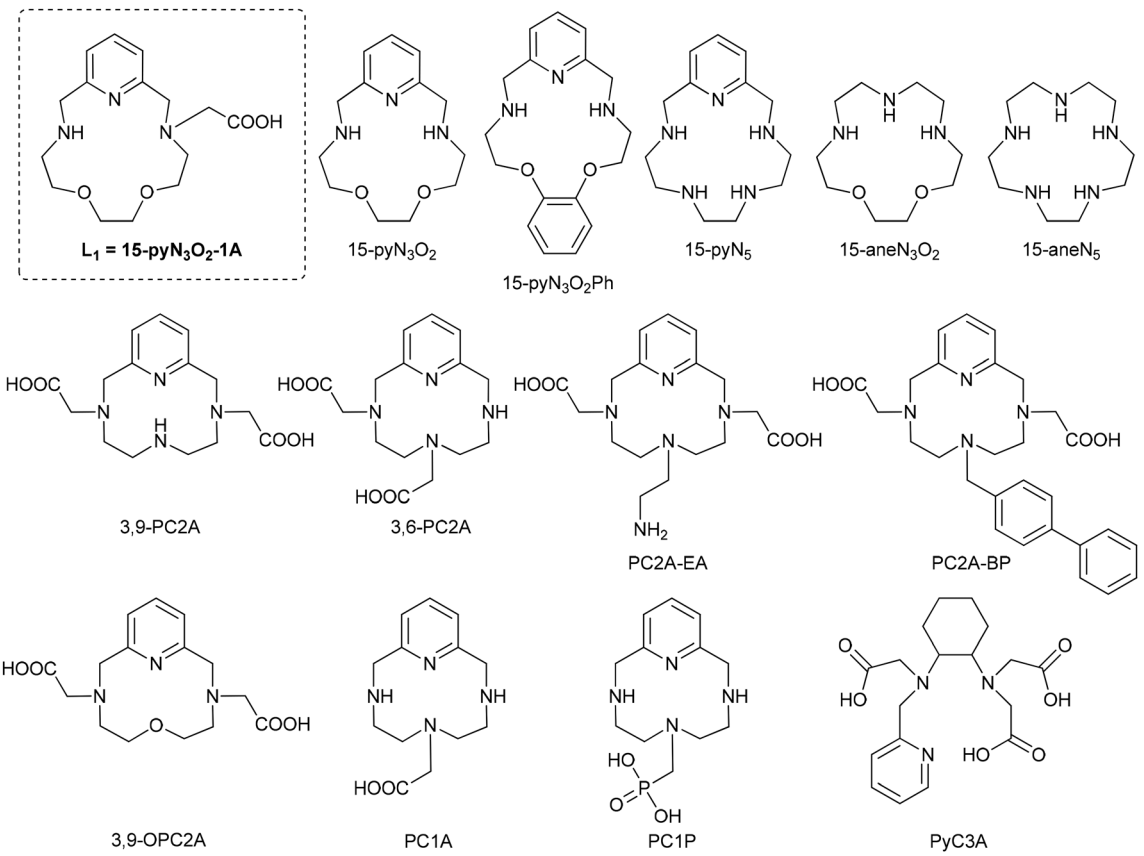

Scheme 1 Structures of **L1** and ligands discussed in the text.

a pyridine and an *ortho*-phenylene unit has been prepared and its Mn(II) complexation has been investigated.[25] This ligand forms a surprisingly flat Mn(II) complex with two coordinated water molecules in the solid state structure; however, due to low stability even under mildly acidic conditions, this complex is unsuitable for further investigation.

In the family of 12-membered macrocycles, pyclen-based 3,9-PC2A and 3,6-PC2A (Scheme 1) and their derivatives are among the most promising ligands for Mn(II) chelation for MRI purposes.[17] Independent of the position of the acetate pendant arms, both 3,9-PC2A and 3,6-PC2A form seven-coordinated Mn(II) complexes which are sufficiently stable and kinetically inert, though they have only one water molecule in the inner coordination sphere, providing lower relaxivity than the above-mentioned 15-membered macrocyclic Mn(II) complexes. The Mn(II) chelates of 3,9-PC2A and 3,6-PC2A possess modest superoxide-dismutase activity as well.[17]

Mn(PC2A-EA), formed with the pyclen-based derivative containing two acetic and one ethylamine pendant arm (Scheme 1), is among the most thermodynamically stable and kinetically inert monohydrated Mn(II) systems.[26] The pH-dependent metal coordination of the ethylamine function, which occurs in the pH range 6–8, results in pH-sensitive relaxivities, making Mn(PC2A-EA) a potential smart CA. Another PC2A derivative bearing a biphenyl pendant arm, PC2A-BP (Scheme 1), also forms a thermodynamically stable and kinetically inert Mn(II) complex.[27] Mn(PC2A-BP) interacts with human serum albumin (HSA) which is accompanied by a remarkable relaxivity increase. This agent could thus be used in angiographic imaging, providing significant MRI signal enhancement in the vasculature.

3,9-OPC2A (Scheme 1) is a less basic analogue of 3,9-PC2A, containing a non-protonable O-atom in the macrocyclic scaffold.[18] Despite a lower ligand basicity, the conditional stability of the Mn(II) complex at pH 7.4 remains unaffected as compared to Mn(3,9-PC2A), while the acid assisted dissociation becomes considerably slower. 3,9-OPC2A could also be efficiently labeled with the PET isotope ^{52}Mn. All these advantageous features make this ligand interesting for further design of bifunctional chelators.

In contrast to PC2A and its derivatives, the monofunctionalized pyclen ligands PC1A and PC1P, which bear a single acetate or phosphonate pendant (Scheme 1), form hexacoordinate and monohydrated Mn(II) complexes (CN = 6; q = 1).[28] Full complexation of Mn(II) occurs at physiological pH and a metal to ligand ratio of 1 : 1; however, the complexes are very labile and undergo oxidation to the Mn^{3+} form.

We should also mention that many linear ligands comprising pyridine or picolinate coordinating functions have also been explored for Mn(II) complexation;[29–31] the ligand PyC3A[32] and its derivatives are likely the most investigated, including clinical trials.

Herein we report a novel 15-membered pyridine-based macrocyclic chelator (**L1**, Scheme 1), where one acetate pendant arm is appended on 15-pyN_3O_2. This modification should lead to higher stability and kinetic inertness, and improved solubility of **MnL1**, all important for potential biological applications. On the other hand, the metal coordination of the acetate group is expected to reduce the hydration number to q = 1, thus resulting in lower relaxivity. We have determined the molecular structure of **MnL1** by single-crystal X-ray diffraction. The protonation constants of the ligand and thermodynamic stability of the complex have been measured in aqueous solution by potentiometry, and kinetic inertness has been assessed in transmetallation experiments of **MnL1** with an excess of Zn^{2+} using T_2 relaxation time measurements. Proton relaxivities, r_1, and the microscopic parameters influencing the relaxivity of **MnL1** have been determined from a combined ^{1}H NMRD and ^{17}O NMR study. Although **MnL1** is not appropriate for further contrast agent development, the comparison of these data to the results on previously reported Mn(II) analogues provides a better understanding of structure–activity relationships in the family of pyridine-containing macrocyclic Mn(II) chelates.

Experimental section

Materials and methods

All solvents (VWR International, Lach-ner, Penta) and chemicals were purchased from commercial sources (Acros Organics, Merck) and used as received. The parent ligand 15-pyN_3O_2 was synthesized as previously described in the literature.[20,33]

Mass spectra were recorded using an LCQ Fleet mass spectrometer (Thermo Scientific, Waltham, MA, USA) equipped with an electrospray source and a three-dimensional (3D) ion-trap detector in the positive/negative mode (Fig. S1†). ^{1}H and ^{13}C NMR spectra (Fig. S2 and S3†) were obtained using a 400-MR NMR spectrometer (Varian, Palo Alto, CA, USA) at 25 °C and 60 °C: ^{1}H 399.95 MHz dimethylsulfoxide-d^6 (DMSO-d^6, residual solvent peak) and ^{13}C 100.60 MHz (DMSO-d^6, residual solvent peak). The multiplicity of the signals is indicated as follows: s – singlet, d – doublet, t – triplet, m – multiplet, and bs – broad singlet. Deuterated solvent DMSO-d^6 (99.9% of D) was purchased from Sigma Aldrich and used as received. The atom numbering scheme used for NMR data interpretation is shown in Scheme 2. The carbon and hydrogen atoms were assigned according to the spectra obtained from two-dimensional correlation experiments ^{1}H–^{1}H *gs*-COSY, ^{1}H–^{13}C *gs*-HMQC (Fig. S4†) and ^{1}H–^{13}C *gs*-HMBC (Fig. S5†).

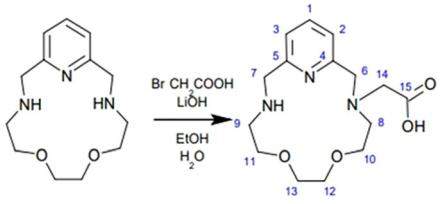

Scheme 2 Synthetic scheme for **L1** preparation and ligand numbering used for NMR data interpretation.

Synthesis

15-pyN_3O_2 (1.70 g, 6.77 mmol) was dissolved in a mixture of EtOH (25 ml) and distilled water (5 ml). Meanwhile, $BrCH_2COOH$ (157.0 mg, 1.13 mmol) and $LiOH{\cdot}H_2O$ (168.0 mg, 4.00 mmol) were dissolved in cooled distilled water (<9 °C) and this resulting solution was added slowly dropwise to a stirred solution of 15-pyN_3O_2. The reaction mixture was then heated to reflux and refluxed for 4 h. Afterwards, the obtained mixture was filtered *via* a glass frit and the filtrate was evaporated to dryness. The residue was dissolved in distilled water and extracted seven times with 50 ml of $CHCl_3$ (the organic phase contained the starting macrocycle 15-pyN_3O_2). The water phase was filtered and evaporated to dryness, and washed several times with hot acetone containing a small amount of 36% hydrochloric acid to dissolve the remaining lithium salt and to get the product in the form of hydrochloride. The residue was then dried under reduced pressure to give a slightly hygroscopic dark orange oil (718 mg of product in the form of hydrochloride/hydrobromide). According to the potentiometric titration of the ligand, the amount of **L1** was 43%, and the rest corresponds to residual solvents and HCl/HBr content, and thus the yield based on $BrCH_2COOH$ was 88.3%. ^{1}H NMR (400 MHz, DMSO-d^6, 60 °C): δ 3.22 (t, $^3J_{HH}$ = 4.9 Hz, 2H, H9); 3.60 (s, 4H, H12/13); 3.64 (m, 2H, H8); 3.78 (m, 2H, H11); 3.85 (t, 2H, $^3J_{HH}$ = 4.9 Hz, H10); 4.19 (s, 2H, H14); 4.40 (bs, 2H, H7); 4.78 (s, 2H, H6); 7.49 (t, 2H, $^3J_{HH}$ = 7.8 Hz H2/H3); 7.95 (t, 1H, $^3J_{HH}$ = 7.8 Hz, H1). ^{13}C NMR (400 MHz, DMSO-d^6, 25 °C): δ 46.83 (C9); 49.49 (C7); 53.71 (C14); 54.54 (C8); 57.5 (C6); 64.13 (C10); 65.11 (C11); 69.53/69.73 (C12/C13); 123.0 (C2/C3); 123.31 (C2/C3); 139.41 (C1); 149.84 (C4); 151.74 (C5); 167.7 (C15). MS *m*/*z* (+): 310.26 ($[\mathbf{L} + H^+]^+$ calcd 310.17), 332.22 ($[\mathbf{L} + Na^+]^+$ calcd 332.16).

Crystal structure determination

Single crystals suitable for X-ray diffraction were prepared by mixing an aqueous/methanol solution of the ligand (c_L = 56 mM) and manganese(II) perchlorate (c_{Mn} = 113 mM) in a 1 : 1.10 Mn/L molar ratio. Several drops of Et_3N were added to this solution. Colorless crystals of the complex were obtained by diffusion of acetone at 25 °C and by additional slow diffusion of Et_2O at 6 °C into the aqua/methanol solution.

X-ray diffraction data were collected on an XtaLAB Synergy-i (Rigaku) diffractometer equipped with a HiPix3000 Bantam detector and a monochromatized microfocus PhotonJet-i CuKα radiation source (λ = 1.54184 Å) at 90 K. The molecular structure of the complex was solved by direct methods and refined by full matrix least squares based on F^2 (SHELXL 2014/07).[34] Program Olex2 1.3 was used for the final refinement.[35] The hydrogen atoms on carbon atoms were fixed into idealized positions (riding model) and assigned temperature factors either $H_{iso}(H) = 1.2U_{eq}$ (pivot atom) for CH and CH_2 moieties or $H_{iso}(H) = 1.5U_{eq}$ (pivot atom) for CH_3 groups. A solvent mask procedure was employed during the refinement process and the residual electron density corresponded to unresolved 1.5H_2O molecules. The molecular and crystal structures of the complex, depicted in Fig. 1 and S3,† were drawn using the Mercury software.[36]

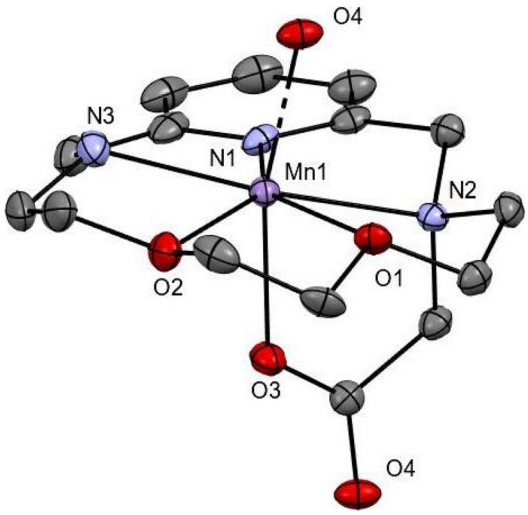

Fig. 1 Molecular structure of the $[\mathbf{MnL1}]^+$ complex unit found in the 1D polymeric structure of $[\mathbf{MnL1}]_n[\mathbf{MnBrCl_3}]_{n/2}{\cdot}2H_2O$.

Thermodynamic stability studies

Metal stock solutions were prepared from the highest analytical-grade chemicals, and their concentration was determined by complexometric titration with standardized Na_2H_2EDTA, using a xylenol orange indicator in the presence of urotropine buffer ($ZnCl_2$ and $MnCl_2$); the Eriochrome black T indicator in the presence of ammonium acetate buffer ($CaCl_2$) or a murexide indicator in ammonium solution ($CuCl_2$). The concentration of the ligand stock solution was determined by pH-potentiometric titrations (the difference between the two inflection points of the ligand titration curve corresponds to two ligand equivalents). To determine the protonation constants of the ligand and stability constants of the metal complexes with selected divalent metal ions, pH-potentiometric titrations were carried out with 0.1 M NaOH using 2 mM ligand solution (protonation constant of the ligand) and then a metal-to-ligand molar ratio of 1 : 1, with a waiting time of 2 minutes between successive points (V_0 = 5 mL). The temperature (25.0 ± 0.1 °C) was controlled with a circulating water bath. The ionic strength was set to I = 0.15 M NaCl. All titrations were performed under a nitrogen atmosphere to avoid the effect of CO_2. Titrations were carried out in the pH range from 1.9 (after the addition of 1 M HCl solution to the starting ligand solution in the titration cell) to pH 11.2 (or until precipitation of the metal hydroxide).

All pH-potentiometric titrations were performed using a 785 DMP Titrino titration workstation with a combined electrode (Metrohm). The $p[H]$ ($p[H] = -\log[H^+]$, concentration in molarity) was measured in each titration with a combined pH glass electrode (Metrohm) filled with 3 M KCl. The electrode was calibrated in hydrogen ion concentration by titration of HCl with KOH in 0.1 M electrolyte solution.[37] A plot of poten-

tial *versus* $p[H]$ allows the determination of the electrode standard potential ($E°$) and the slope factor (f).

The protonation constants of the ligand ($\log K_i^H$) are defined as follows:

$$K_i^H = \frac{[H_iL]}{[H_{i-1}L][H^+]}$$

where i = 1, 2... and $[H_{i-1}L]$ and $[H^+]$ are the equilibrium concentrations of the ligand (i = 1), its protonated forms (i = 2,...) and the hydrogen ion. The stability constants of metal complexes are defined as follows:

$$K_{ML} = \frac{[ML]}{[M][L]}$$

$$K_{MH_iL} = \frac{[MH_iL]}{[MH_{i-1}L][H^+]}.$$

For the calculation of equilibrium constants, the HYPERQUAD program was used.[38] The number of fitted data pairs was between 230 and 280. The ionic product of water at 25 °C and 0.1 M ionic strength is pK_w = 13.77.[39] Fixed values were used for pK_w, ligand acidity constants and total concentrations of the metal, ligand, and acid. All values and errors (one standard deviation) reported are at least the average of three independent experiments.

Sample preparation

MnL1 complex samples for kinetic and relaxometry studies have been prepared by mixing $MnCl_2$ and **L1** solutions of known concentrations in a ratio of 1 : 1.05 and by adjusting the pH to 7.4. Mn(II) concentration in each sample was checked by bulk magnetic susceptibility measurements.

Kinetic studies

The transmetalation reaction of **MnL1** (1.4 mM solution) was monitored in the presence of 10, 20, 30, 40 and 50 molar equivalents of Zn(II) ions, by measuring water proton T_2 relaxation times (60 MHz) as a function of time at 25 °C and in 0.15 M NaCl, in the pH range 4.9–6.1 (4.9; 5.0; 5.2; 5.5; 5.7; 6.1). To control pH, 50 mM *N*-methyl-piperazine (pH 4.9–5.5) or 50 mM MES buffer (pH 5.7–6.1) was used. No oxidation of the sample was observed.

Relaxation properties

At 60 MHz, ^{1}H longitudinal (T_1) and transverse (T_2) relaxation times were measured with a Bruker Minispec MQ-60 NMR analyzer. The temperature was set to 25.0 °C and controlled with a circulating water bath. T_1 and T_2 values were determined, respectively, by the inversion recovery method ($180° - \tau - 90°$) and the Carl–Purcell–Meiboom–Gill (CPMG) spin-echo pulse sequence. pH-Dependent relaxivities (pH 1.75–11.8) were acquired at a **MnL1** concentration of 2 mM, and the pH was adjusted by 0.045 M MES (2-(4-morpholino)ethane-sulfonic acid), HEPES (4-(2-hydroxyethyl)piperazine-1-ethanesulfonic acid), DMP (dimethyl piperazine), or NMP (*N*-methyl piperazine) buffers.

The ^{1}H NMRD profiles of aqueous **MnL1** solution ($c_{Mn^{2+}}$ = 0.99 mM; pH = 7.23) were recorded at 25 and 37 °C on a SMARTracer Fast Field Cycling NMR relaxometer (Stelar; 0.00024–0.24 T, 0.01–10 MHz ^{1}H Larmor frequency) and a WP80 NMR electromagnet adapted to variable-field measurements (Bruker; 0.47–1.88 T, 20–80 MHz ^{1}H Larmor frequency). The temperature was maintained by a gas flow and monitored using a VTC91 temperature control unit, based on previous calibration with a Pt resistance temperature probe.

^{17}O NMR measurements

Variable-temperature ^{17}O NMR measurements of an aqueous solution of **MnL1** (c_{MnL} = 4.01 mmol kg^{-1}, pH = 7.39) were performed using a Bruker Avance III 400 MHz spectrometer (9.4 T, 54.2 MHz) in the temperature range of 5–75 °C. The temperature was calculated after calibration with ethylene glycol and MeOH. Acidified water ($HClO_4$, pH = 3.3) was used as a diamagnetic reference. The ^{17}O transverse relaxation times (T_2) were obtained using the CPMG spin-echo technique. To eliminate susceptibility contributions to the chemical shift, the sample was in a glass sphere placed in a 10 mm NMR tube. To improve sensitivity, ^{17}O-enriched water (11.10% $H_2{}^{17}O$, Cortecnet) was added to the solution to yield approximately 1% ^{17}O enrichment.

The ^{17}O NMR and NMRD data have been treated according to the Solomon–Bloembergen–Morgan theory of paramagnetic relaxation.[40] The least squares fit was performed using Visualiseur/Optimiseur running on a MATLAB 8.3.0 (R2014a) platform.

Results and discussion

Synthesis

The 15-pyN_3O_2 macrocycle was obtained first *via* template synthesis as previously described.[20,33] Two procedures were tested for the preparation of **L1**.

The first one used $BrCH_2COOH$ and 15-pyN_3O_2 in a molar ratio of 1 : 6; lower excess of 15-pyN_3O_2 led to higher amounts of the disubstituted side-product. The reaction was performed in MeOH and the product was purified by successive anion and cation exchange chromatography. The resulting product, obtained in zwitterionic form, contained *ca.* 5–20% of the disubstituted side-product (based on NMR analysis and MS). The reaction yield (50–60%) and the purity (ranging from 60 to 90%) were strongly dependent on the temperature during $BrCH_2COOH$ addition (room temperature *vs.* 60 °C), the speed and the form of $BrCH_2COOH$ addition (in the form of solid or solution, and the addition of the solution takes place *via* a dropping funnel or linear pump) and the reflux time ranging from 1.5 to 12 h. Further optimization seemed difficult in the case of this procedure.

The second synthetic route was based on a procedure previously described in the literature for the preparation of mono-*N*-substituted cyclam (1,4,8,11-tetraaza-cyclotetradecane) using $LiOH{\cdot}H_2O$ and a large excess of the macrocycle.[41] Therefore, we used a $BrCH_2COOH$/15-pyN_3O_2 molar ratio of 1 : 7, and

according to NMR and MS/HPLC characterization, this synthetic procedure led to high ligand purity without side product (s). Attempts (*e.g.* dissolving the product in a minimum amount of distilled water and HCl, followed by the addition of acetone/ether) to obtain a solid crystallized ligand were unsuccessful. Therefore, solvents were evaporated under reduced pressure to obtain the ligand as an orange oil. Subsequent potentiometric titration of this product revealed the amount of **L1** to be 43%, and the rest corresponding to HCl/HBr and the water content. The calculated yield, based on $BrCH_2COOH$ and the 43% purity, was 88.3% which can be considered as high and superior to that of the above-described first approach.

Crystal structure determination

For single-crystal preparation, a solution of manganese perchlorate was mixed with ligand solution in $MeOH/H_2O$ (1/1) in a molar ratio of 1 : 1 (before the addition of the manganese(II) solution, a small amount of triethylamine in methanol was dropped to the ligand solution to adjust the pH and to deprotonate the ligand). Only a few crystals were suitable for X-ray diffraction analysis. Many attempts were made, by using various solvents, to prepare single crystals of the complex with coordinated water molecules. They all gave crystals of very bad quality; nevertheless, the polymeric structure could be always confirmed. In the crystal structure of $[\mathbf{MnL1}]_n[\mathbf{MnBrCl_3}]_{n/2}\cdot 2H_2O$ (**1**), the $[\mathbf{MnL1}]^+$ units were found to form a 1D polymeric chain in which the pendant carboxylate group acts as a bridging ligand between two $[\mathbf{MnL1}]^+$ units (Fig. 1). The positive charge is compensated by $[MnBrCl_3]^{2-}$ counter anions.

For each $[\mathbf{MnL1}]^+$ unit of the 1D polymeric chain, the coordination sphere has a pentagonal bipyramidal geometry, with the three nitrogen and two oxygen atoms of the macrocycle coordinated in the equatorial plane and the two oxygen atoms of the acetate pendant arms in apical positions, resulting in a coordination number of seven for Mn(II). The crystal data and structural refinements are summarized in Table 1.

Among all Mn–N distances (2.298 and 2.355 Å), the Mn1–N1(pyridine) distance (2.216 Å) is the shortest and the Mn1–N2 distance (2.355 Å) is the longest, where N2 bears the acetate pendant arm. The bond distances between the oxygen atoms of the macrocyclic cavity and the central Mn are 2.280 and 2.329 Å. The distances between the oxygen atoms of the pendant arm (O3/O4) and the central Mn atom are *ca.* 0.1–0.2 Å shorter compared to the Mn–O1/O2 distances as well as all other distances (see Table 2), and thus, the pentagonal bipyramidal geometry is slightly axially compressed.

The positive charge of the 1D coordination polymer is compensated by $[MnBrCl_3]^{2-}$ anions (Br^- anions are retained from the ligand synthesis) which have a distorted tetrahedral structure. Mn–Br distances are *ca.* 0.1 Å longer in comparison with Mn–Cl ones. Moreover, this anion has occupational disorder because the Br atom is situated in two positions of the tetrahedron (occupancy factors of 0.55 and 0.45).

Furthermore, in the crystal structure of **1**, there are two co-crystallized solvent water molecules for every $[\mathbf{MnL1}]^+$ unit which form hydrogen bonds between each other (O–H···$O_{(water)}$), with the carboxylate bridge (O–H···$O_{(COOH)}$), the macrocyclic NH group (N–H···$O_{(water)}$) or the Cl atom from the $[MnBrCl_3]^{2-}$ anion (O–H···Cl); see Table S1 and Fig. S6 in the ESI.† One of the water molecules also has positional disorder.

Table 1 Crystal data and structural refinements for the studied 1D polymeric complex **1** ($[MnL1]_n$ $[MnBrCl_3]_{n/2}\cdot 2H_2O$)

Compound	**1**
Formula	$C_{30}H_{50}BrCl_3Mn_3N_6O_{11}$
M_r	1021.84
Temperature (K)	90.15
Wavelength (Å)	1.54184
Crystal system	Orthorhombic
Space group	*Pnma*
a (Å)	11.7529(2)
b (Å)	20.8862(4)
c (Å)	18.2988(3)
α (°)	90
β (°)	90
γ (°)	90
V, Å^3	4491.87(14)
Z	4
$D_{calc.}$ (g cm^{-3})	1.511
μ (mm^{-1})	9.923
$F(000)$	2084
$R(int)^a$	0.0526
Data/restraints/parameters	4181/6/256
Completeness to θ (%)	99.4
Goodness-of-fit on F^2	1.046
R_1, $wR_2{}^b$ ($I > 2\sigma(I)$)	0.0532/0.1485
R_1, $wR_2{}^b$ (all data)	0.0551/0.1505
Largest diff. peak and hole (A^{-3})	1.067 and −0.849
CCDC	2244643

$^a R_{int} = \sum|F_o{}^2 - F_{o,mean}{}^2|/\sum F_o{}^2$. $^b R_1 = \sum(||F_o| - |F_c||)/\sum|F_o|$; $wR_2 = [\sum w(F_o{}^2 - F_c{}^2)^2/\sum w(F_o{}^2)^2]^{1/2}$.

Table 2 Selected interatomic distances [Å] and angles [°] in the complex cation $[\mathbf{MnL1}]^+$ of complex **1**

Distances	
Mn1–N1	2.216(3)
Mn1–N2	2.355(3)
Mn1–N3	2.298(3)
Mn1–O1	2.329(2)
Mn1–O2	2.280(2)
Mn1–O3	2.159(2)
Mn1–O4	2.134(2)
Angles	
N1–Mn1–N2	71.90(10)
N1–Mn1–N3	72.66(11)
N3–Mn1–O2	73.59(10)
O1–Mn1–O2	70.37(9)
N2–Mn1–O1	73.70(9)
O3–Mn1–O4	165.66(10)

Equilibrium studies in aqueous solution. The stepwise protonation constants of **L1** and stability constants formed with Mn(II), Zn(II), Cu(II) and Ca(II) ions have been determined using potentiometry. Complex formation was fast for all systems and allowed direct titrations. Titration curves are given in Fig. S7† and the calculated constants are shown and compared to those of selected macrocyclic ligands in Tables 3 and 4.

The first protonation constant, $\log K_{H1}$, is similar for **L1** and the parent ligand 15-pyN_3O_2, but it is lower than $\log K_{H1}$

Table 3 Stepwise protonation constants of **L1** and other selected ligands obtained from potentiometry (I = 0.15 M NaCl; 25 °C)

	$\log K_1^H$	$\log K_2^H$	$\log K_3^H$	$\log K_4^H$
L1	8.86(1)	8.03(1)	1.9(1)	
15-pyN_3O_2 [a]	8.82	7.8		
15-pyN_5 [a]	9.40[a] (9.43[b]; 9.11[c])	8.54[a] (8.80[b]; 8.82[c])	5.28[a] (5.28[b]; 5.27[c])	
15-pyN_3O_2Ph[d]	8.53	7.63		
3,9-PC2A	12.25[e]/12.50[f]	5.97[e]/5.75[f]	3.47[e]/3.28[f]	1.99[e]/2.38[f]
3,6-PC2A	10.72[e]/10.31[g]	8.37[e]/8.59[g]	3.81[e]/3.92[g]	1.26[e]/1.56[g]
PC2A-EA[h]	11.34	8.93	6.91	1.97
PC2A-BP[i]	10.45	6.93	2.36	1.64
3,9-OPC2A[j]	7.73	7.66	2.13	
PC1A[k]	10.47	8.71	2.79	
PC1P[k]	11.84	9.64	6.23	0.99

[a] Ref. 20 (0.1 M NMe_4Cl). [b] Ref. 21 (0.1 M $NaClO_4$). [c] Ref. 22 (0.1 M $NaClO_4$). [d] Ref. 25 (0.15 M NaCl). [e] Ref. 17 (0.15 M NaCl). [f] Ref. 43 (0.1M KCl). [g] Ref. 17 (1.0 M NaCl). [h] Ref. 26 (0.15 M NaCl). [i] Ref. 27 (0.15 M NaCl). [j] Ref. 18 (0.15 M NaCl). [k] Ref. 28 (0.1 M NMe_4Cl).

for 15-pyN_5 or the other cyclic ligands (Table 3). This lower basicity is related to the electron-withdrawing effect of the highly electronegative oxygen atoms in the macrocyclic scaffold. The second protonation constants are similar for **L1** and 15-pyN_3O_2, while the third constant of **L1** corresponds to the additional acetate function. Protonation of the pyridine unit is not observable above pH 1.9.

According to the stability constants (Table 4), the most stable complex is formed with Cu(II), and then the $\log K_{ML}$ values decrease in the order Cu(II) > Zn(II) > Mn(II) > Ca(II). Protonated **HML1** complexes exist for all four metals investigated, while a hydroxo complex is detected only for **CuL1** at basic pH.

As expected, the modification with the acetate pendant arm leads to higher stability for **L1** *vs.* 15-pyN_3O_2 analogues, with an increase of *ca.* 4 units in the $\log K_{ML}$ values. Recently, an empirical approach, based on various structural descriptors, has been proposed to estimate stability constants for Mn(II) complexes.[42] Considering the stabilization effect of the additional acetate in comparison with the parent 15-pyN_3O_2, this method predicts $\log K_{ML}$ = 9.64 for **MnL1**, *ca.* 1.4 units lower than the experimental value. For a more direct comparison of MnL stabilities between ligands with different protonation constants, pMn (pMn = −log[Mn(II)]$_{free}$ at pH 7.4, $c_{Mn} = c_{lig} = 10^{-5}$ M) was calculated for **MnL1** and compared to those of other systems (Table 4). This comparison reflects again an important stability increase brought by the introduction of the additional carboxylate donor in **L1**. Nevertheless, the stability of **MnL1** remains low as compared to Mn(II) complexes of 12-membered pyclen derivatives (Table 4), mainly because of the too large size of the macrocyclic cavity and the lower number of pendant acetates.

The species distribution curves calculated for **MnL1** with the stability constants as obtained by pH-potentiometry were corroborated with pH-dependent ^{1}H-relaxometry data (Fig. 2). Full complex formation is achieved above pH 6.5. The relaxivity decrease observed between pH 6 and 7 might be the consequence of a small quantity of an additional protonated species present, not detectable in the pH potentiometric titration. From pH 7 and up to pH 11, **MnL1** exhibits constant relaxivity (2.30 mM^{-1} s^{-1}, at 0.49 T and 25 °C), evidencing the lack of substantial hydrolysis. Below pH 6, the relaxivity increase corresponds to complex protonation followed by dissociation, to reach r_1 = 6.7 mM^{-1} s^{-1}, characteristic of $[Mn(H_2O)_6]^+$.[44]

Dissociation kinetics

The resistance of Mn(II) complexes to dissociation or transmetalation by endogenous ions such as Cu(II) or Zn(II) is another important parameter for safe *in vivo* administration. In order to describe the kinetic inertness of **MnL1**, we have evaluated the rate of transmetalation in the presence of Zn(II) which forms more stable complexes than Mn(II), and thus can induce dissociation. Dissociation was followed by monitoring Mn(II) release by water proton T_2 measurements, at pH 4.9–6.1, in the presence of 10–50 fold excess of Zn(II) to ensure pseudo-first order conditions.

The observed dissociation rate constants, k_{obs}, increase with an increase in H^+ ion concentration (Fig. 3), while remain independent of the Zn(II) concentration (Fig. S8†).

In the excess of the exchanging metal, the reaction is of pseudo-first order, and the rate is proportional to the total **MnL1** concentration (eqn (1)), where k_{obs} is the pseudo-first order rate constant.

$$-\frac{d[MnL]_{tot}}{dt} = k_{obs}[MnL]_{tot} \quad (1)$$

In general, different dissociation pathways can co-exist, implying the participation of protons and/or the exchanging metal ion,[45] as illustrated in Fig. 4.

Based on this scheme, the overall dissociation rate can be given using eqn (2) (for clarity, charges of complexes are omitted).

$$\begin{aligned}-\frac{d[MnL]_{tot}}{dt} &= k_{MnL}[MnL] + k_{MnHL}[MnHL] \\ &+^{H} k_{MnHL}[MnHL][H^+] +^{Zn} k_{MnL}[ZnLMn] \\ &+^{Zn} k_{MnHL}[MnHL][Zn^{2+}]\end{aligned} \quad (2)$$

Here the first and second terms correspond to the spontaneous dissociation of the non-protonated and the monoprotonated complexes, respectively, the third term describes the proton-assisted dissociation of the monoprotonated complex, and the last two terms refer to the metal-assisted dissociation

Table 4 Stability and protonation constants of Ca(II), Mn(II), Zn(II) and Cu(II) complexes of **L1** and other selected ligands (I = 0.15 M NaCl; 25 °C) together with *p*Mn values

Constant	Ca(II)	Mn(II)	Zn(II)	Cu(II)
L1				
$\log K_{ML}$	5.51(2)	11.06(2)	13.12(1)	15.86(2)
$\log K_{HML}$	6.37(2)	3.82(3)	2.80(6)	2.67(3)
$\log K_{ML(OH)}$				−9.7(1)
*p*Mn[a]		6.95		
15-pyN$_3$O$_2$[b]				
$\log K_{ML}$	2.04	7.18	8.58	13.91
$\log K_{ML(OH)}$	−11.92	−11.69	−10.31	−8.34
$\log K_{ML(OH)2}$				−12.57
*p*Mn		5.28		
15-pyN$_5$[b]				
$\log K_{ML}$	2.97	10.89 (11.64[c], 11.12[d])	16.27	21.84
$\log K_{HML}$		4.27 (4.20[c], 4.51[d])	2.45	
$\log K_{ML(OH)}$		−11.52 (11.54[c])	−11.18	−12.30
*p*Mn		6.37 (6.60[c], 6.59[d])		
15-pyN$_3$O$_2$Ph[e]				
$\log K_{ML}$	1.85	5.62	7.70	13.97
$\log K_{ML(OH)}$		−10.50	−9.62	−8.95
*p*Mn[a]		5.04		
3,9-PC2A[f]				
$\log K_{ML}$	9.92	17.09	19.49	23.58[g]
$\log K_{HML}$	5.08	2.14	2.74	2.12[g]
*p*Mn		8.64		
3,6-PC2A[f]				
$\log K_{ML}$	9.57	15.53	20.37	24.09[g]
$\log K_{HML}$	5.27	3.06	2.36	2.37[g]
*p*Mn		8.09		
PC2A-EA[h]				
$\log K_{ML}$		19.01		
$\log K_{HML}$		6.88		
$\log K_{H2ML}$		2.50		
*p*Mn		9.27		
PC2A-BP[i]				
$\log K_{ML}$	7.94	14.86	18.05	22.30
$\log K_{HML}$			1.71	1.04
*p*Mn		8.35		
3,9-OPC2A[j]				
$\log K_{ML}$	8.27	13.03	14.81	18.41[j]
$\log K_{HML}$		2.40	2.08	1.92[j]
$\log K_{ML(OH)}$		−11.49	−10.95	−10.50
*p*Mn		8.69		
PC1A[k]				
$\log K_{ML}$	6.04	11.54	17.01	18.62
$\log K_{HML}$	7.39	4.95	3.03	2.09
$\log K_{ML(OH)}$			10.46	11.35
*p*Mn		8.10		
PC1P[k]				
$\log K_{ML}$	6.85	14.06	19.66	22.63
$\log K_{HML}$		5.35	5.19	4.89
$\log K_{ML(OH)}$		−11.97	12.33	13.12
*p*Mn		8.30		

[a] Calculated using *p*Mn = −log[Mn], $c_{Mn(II)} = c_{lig}$ = 0.01 mM at pH 7.4. [b] Ref. 20 (0.1 M NMe_4Cl). [c] Ref. 21 (0.1 M $NaClO_4$). [d] Ref. 22 (0.1 M $NaClO_4$). [e] Ref. 25 (0.15 M NaCl). [f] Ref. 17 (0.15 M NaCl). [g] Ref. 17 (1.0 M NaCl; determined by simultaneous fitting of the pH-potentiometric and UV-Vis data). [h] Ref. 26 (0.15 M NaCl). [i] Ref. 27 (0.15 M NaCl). [j] Ref. 18 (0.15 M NaCl). [k] Ref. 28 (0.1 M NMe_4Cl).

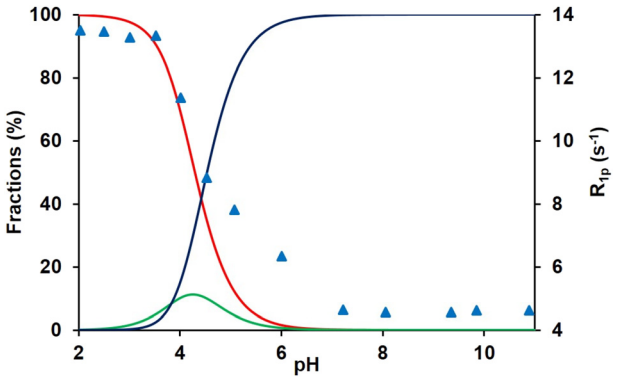

Fig. 2 Species distribution diagram of the Mn(II)–**L1**–H^+ system ([Mn(II)] = [**L1**] = 2.01 mM; solid lines; red = [$Mn(II)_{free}$], green = [MnHL1], blue = [**MnL1**]) and r_1 obtained as a function of pH at 1.41 T, 60 MHz (T = 25 °C and I = 0.15 M NaCl; blue triangles).

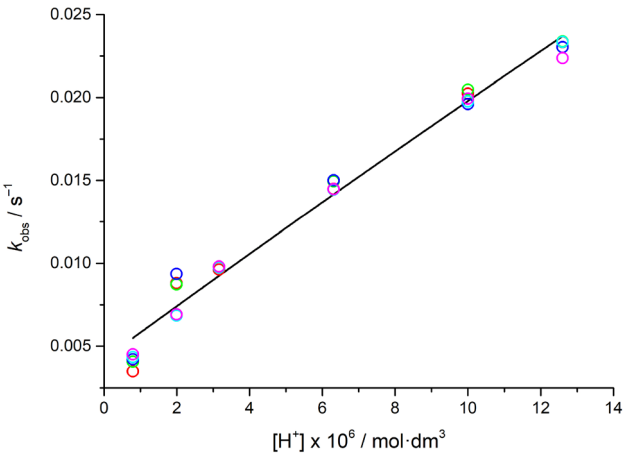

Fig. 3 Dependence of the observed dissociation rate constants of **MnL1** (1.4 mM) on the proton concentration at Zn^{2+} concentrations of 10 (red), 20 (green), 30 (blue), 40 (light blue) and 50 mM (magenta).

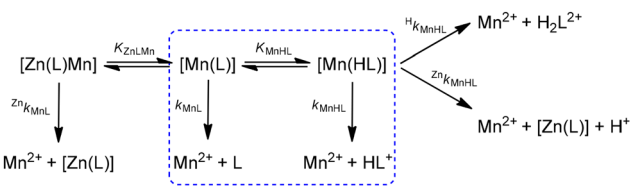

Fig. 4 Possible dissociation pathways of **MnL1**. The pathways having a real contribution to the overall dissociation, as indicated by the fit of the observed rate constants, are highlighted by a blue dashed line.

of the non-protonated and the monoprotonated **MnL1** complex. $[MnL]_{tot}$ is the total concentration of Mn(II) chelates ($[MnL]_{tot}$ = [MnL] + [MnHL] + [ZnLMn]). Since no Zn(II) dependence is observed, only the spontaneous and the proton-assisted dissociation pathways are considered, and thus the observed rate constants can be expressed as in eqn (3), with $k_0 = k_{MnL}$, $k_1 = k_{MnHL}{\cdot}K_{MnHL}$, and $k_2 = {}^{H}k_{MnHL}{\cdot}K_{MnHL}$.

$$k_{obs} = \frac{k_0 + k_1[H^+] + k_2[H^+]^2}{1 + K_{MHL}[H^+]} \quad (3)$$

The rate constants were thus fitted to eqn (3) (Fig. 3), and the calculated parameters are listed in Table 5. In the fit, the protonation constant, K_{MnHL}, was fixed to the value obtained

Table 5 Rate and equilibrium constants and half-lives of dissociation (pH 7.4) of selected Mn(II) complexes

	k_0 (s^{-1})	k_1 (M^{-1} s^{-1})	k_2 (M^{-2} s^{-1})	k_3 (M^{-1} s^{-1})	k_4 (M^{-2} s^{-1})	log K_{MnHL}[a]	$t_{1/2}$ (h)	Metal used in transmetalation
L1	$(4.1 \pm 0.3) \times 10^{-3}$	1691 ± 41				3.82	2.8 min	
15-pyN$_5$ [b]		423	1.0×10^7		1.7×10^4	4.27	11.0	Zn(II)
3,9-PC2A[c]		221 ± 5		$(3.6 \pm 0.5) \times 10^{-2}$		2.14	21.0	Zn(II)
3,6-PC2A[c]		70 ± 1	$(1.5 \pm 0.4) \times 10^5$	$(2.6 \pm 0.7) \times 10^{-2}$		3.06	63.2	Cu(II)
PC2A-EA[d]		0.6				6.88	8.00×10^3	Cu(II)
PC2A-BP[e]		16.9 ± 0.2					286.2	Cu(II)
3,9-OPC2A[f]	$(8.6 \pm 1.1) \times 10^{-6}$	2.81 ± 0.07				(2.40)	21.9	Cu(II)
PC1A[g]		2020 ± 40	$(8.0 \pm 0.3) \times 10^7$			4.95	2.4	Cu(II)

[a] Obtained *via* pH-potentiometric titration and fixed during the calculations. [b] Ref. 20. [c] Ref. 17. [d] Ref. 26. [e] Ref. 27. [f] Ref. 18. [g] Ref. 28.

from pH-potentiometric titrations. The k_0 value determined is $(4.1 \pm 0.3) \times 10^{-3}$ s^{-1} which shows that the spontaneous dissociation of **MnL1** has a significant contribution to the overall dissociation, even if the fitted curve indicates that the k_0 value is overestimated. The other important pathway is the spontaneous dissociation of the monoprotonated complex, characterized by $k_1 = (1691 \pm 41)$ M^{-1} s^{-1}. k_2 was fixed to zero during the fitting procedure; otherwise, very low values were obtained with large errors, indicating that the proton-catalyzed dissociation of the monoprotonated complex is negligible in the pH range investigated. We should note that the pH range of this study is relatively limited (4.9–6.1; below 4.9 the dissociation becomes too fast to be followed by relaxometry), which likely leads to higher errors on the rate constants calculated. When the observed rate constants have been analyzed by also fitting the protonation constant of the complex, K_{MnHL}, we obtained an unreasonably high value, 10-fold higher than that calculated from the potentiometric data, and on the other hand, k_0 was about 50% smaller in this fit. We believe that the potentiometric determination of the protonation constant is highly reliable; therefore, we prefer keeping it fixed in the fit.

Overall, the introduction of an acetate pendant arm in the ligand results in slower dissociation for **MnL1** as compared to the 15-pyN$_3$O$_2$ analogue, for which the dissociation was too fast and not measurable using relaxometry. Similarly, very fast dissociation was reported for Mn(15-pyN$_3$O$_2$Ph).[25] Interestingly, the Mn(II) complex of the 15-membered analogue 15-pyN$_5$ undergoes slower proton-assisted dissociation (k_1 is four times lower than for **MnL1**).[20] For Mn(15-pyN$_5$), as well as for pyclen derivative complexes, k_0 could not be assessed; it had to be fixed to zero in the fitting; otherwise small values were obtained with large errors (Table 5). For the pyclen derivatives, the zinc-assisted pathway that proceeds *via* the formation of a dinuclear Zn(L)Mn complex, characterized by k_3, also contributes to a small extent to the overall dissociation, while zinc-assisted dissociation of the monoprotonated complex characterized by k_4 was found for Mn(15-pyN$_5$).[20]

The dissociation half-life of **MnL1** was estimated at pH 7.4 and compared to those of other complexes (Table 5). **MnL1** has the shortest half-life, related to the important contribution of spontaneous dissociation. Since in most of the other cases this pathway was not considered, this comparison should be taken with caution. Nevertheless, the high lability of **MnL1** is obvious. In the family of these fifteen-membered macrocycles which form seven-coordinate pentagonal-bipyramidal complexes, the presence of labile Mn–ether O bonds disfavors kinetic inertness, as it was also found previously in comparing the dissociation of Mn(15-pyN$_5$) and Mn(15-pyN$_3$O$_2$), where the all-nitrogen-donor ligand better prevented decomplexation.[10,20] The situation might be different for more rigid 12-membered macrocycles. For instance, the rate constant characterizing the acid-assisted dissociation decreased by two orders of magnitude for MnOPC2A in comparison with the N-containing 3,9-PC2A analog.[17,18] On the other hand, **MnL1** has the slowest dissociation among Mn(II) complexes of 15-membered N$_3$O$_2$ macrocyclic ligands, pointing out the beneficial effect of the acetate pendant arm.

^{17}O NMR and ^{1}H NMRD

The nuclear relaxation enhancement effect of paramagnetic metal ions is described by Solomon–Bloembergen–Morgan theory of paramagnetic relaxation.[4] This model relates relaxivity to the dynamic and structural parameters of the metal complexes. The ^{1}H NMRD profiles represent the magnetic field dependency of relaxivity and are crucial to determining microscopic parameters governing relaxivity and distinguishing between different relaxation mechanisms. ^{1}H NMRD measurements are often complemented by ^{17}O NMR data that give direct access to the water exchange process, important for the description of relaxivity.

Variable-temperature transverse ^{17}O relaxation times were measured in aqueous **MnL1** solution at pH 7.4, where the complexation is complete (Fig. 2). Longitudinal ^{17}O relaxation rates and chemical shifts were also measured, but because of large errors, they were not further analyzed. The rate, k_{ex}^{298}, and the activation enthalpy, $\Delta H^{\ddagger}$, and the entropy, $\Delta S^{\ddagger}$, of water exchange can be determined from the temperature dependence of the ^{17}O transverse relaxation rates, which are dominated by the scalar mechanism.[47] In the slow exchange regime, where the $1/T_{2r}$ values increase with an increase in temperature, only water exchange is important for transverse ^{17}O relaxation. In the fast exchange regime, where the $1/T_{2r}$ values decrease with an increase in temperature, transverse ^{17}O relaxation rates depend also on electronic relaxation and

the hyperfine coupling constant $A_O/\hbar$; however, this regime is not observable for **MnL1**.

^{1}H NMRD profiles were recorded at 25 and 37 °C in the magnetic field range 0.01–80 MHz (Fig. 5). The reduced transverse ^{17}O relaxation rates were simultaneously fitted with ^{1}H NMRD data according to Solomon–Bloembergen–Morgan theory (equations for this analysis are given in ESI†). Fitted parameters are summarized in Table 6 and compared to selected seven-coordinate Mn(II) complexes and $[Mn(H_2O)_6]^{2+}$.

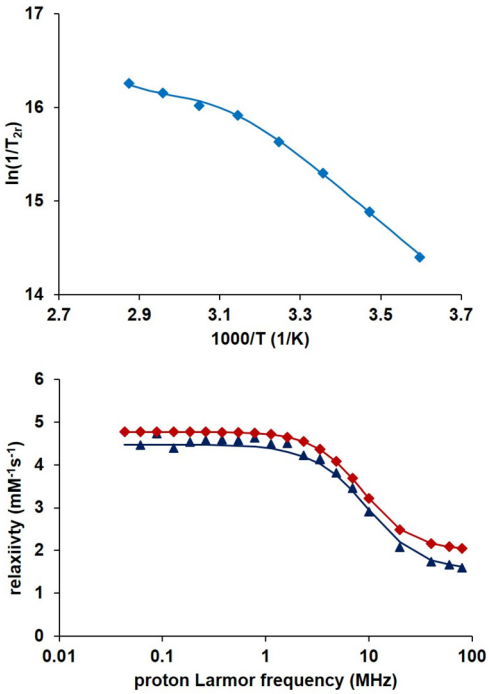

Fig. 5 Top: temperature dependence of the reduced ^{17}O transverse relaxation rate of **MnL1** at 9.4 T and pH 7.4. Bottom: ^{1}H NMRD profiles at 25 (red) and 37 °C (blue) measured for **MnL1**; c_{MnL1} = 1 mM at pH = 7.4. Full lines represent the best simultaneous fit of ^{17}O NMR and ^{1}H NMRD data.

The shape of the ^{1}H NMRD curves corresponds to low-molecular-weight complexes and shows one dispersion between 1 and 10 MHz as has been previously described for other complexes except $[Mn(H_2O)_6]^{2+}$.[48,49] The hydration number of **MnL1** was assumed to be q = 1 for a total coordination number of CN = 7, based on the X-ray crystal structure. In aqueous solution, the oxygen of one acetate pendant arm which coordinates to Mn(II) to form a 1D polymeric chain in the solid-state is expected to be replaced by a water molecule to complete the coordination sphere of Mn(II). As proposed by Gale *et al.*,[50] the ^{17}O T_2 values can also give an estimate of the hydration number, provided the $1/T_{2r}$ *vs.* temperature curve has a maximum. As **MnL1** is in the slow exchange regime in the entire temperature range studied, this approach to assess the hydration number is not applicable. We note also that the lack of a fast exchange regime prevents the fit of the scalar coupling constant, $A_O/\hbar$, as well which was fixed to the value of 38.6 MHz.[20] On the other hand, the relaxivity of **MnL1** is comparable to those of other monohydrated Mn(II) chelates, and thus they support q = 1 (Table 7), but it is about 40% lower for **MnL1** than for the bishydrated Mn(15-pyN$_3$O$_2$) (Table 6). A semi-empirical method was recently proposed for the estimation of the hydration number for Mn(II) complexes,[51] based on the molecular weight of the chelate and the low field relaxivity (0.01 MHz if the NMRD profile has one dispersion). This method gave q = 0.8, in accordance with the assumed q = 1.

The water exchange rate calculated for **MnL1**, k_{ex}^{298} = 0.45 × 10^7 s^{-1}, is higher than the value previously obtained for Mn(15-pyN$_3$O$_2$), but it remains one of the lowest ever observed for a Mn(II) chelate; it is slightly below that reported for Mn(15-pyN$_3$O$_2$Ph) (k_{ex}^{298} = 0.64 × 10^7 s^{-1}).[25]

We note that the negative activation entropy, $\Delta S^{\ddagger}$, is in accordance with a dissociative water exchange mechanism, as we expect for a seven-coordinated Mn(II) complex.

Given the slow water exchange of **MnL1**, and thus the lack of a fast exchange regime, in our analysis, the electronic relaxation parameters are determined by the NMRD data, essentially at low magnetic fields. These low field relaxivities are

Table 6 Relaxivities and best-fit parameters obtained from the simultaneous analysis of ^{17}O NMR and ^{1}H NMRD data for **MnL1** compared with those for other 15-membered Mn(II) chelates and the hexaaqua Mn(II) ion

Parameter[e]	[Mn(**L1**)(H$_2$O)]$^+$	[Mn(15-pyN$_3$O$_2$)(H$_2$O)$_2$]$^{2+}$ [a]	[Mn(15-pyN$_5$)(H$_2$O)$_2$]$^{2+}$ [a]	[Mn(15-pyN$_3$O$_2$Ph)(H$_2$O)$_2$]$^+$ [b]	[Mn(H$_2$O)$_6$]$^{2+}$ [c]
CN/q	7/1	7/2	7/2	7/2	—
r_1 at 25/37 °C /mM^{-1} s^{-1} (20 MHz)	2.45/2.08	4.48/3.61	3.56/3.13	5.16/—	8.36/—
k_{ex}^{298}/10^7 s^{-1}	0.45 ± 0.02	0.38	6.9	0.64 ± 0.05	2.1
$\Delta H^{\ddagger}$/kJ mol^{-1}	28.1 ± 2.1	35.3	37.7	34.0 ± 3	32.9
$\Delta S^{\ddagger}$/J mol^{-1} K^{-1}	−23 ± 6	−1.0	+32	−1.0 ± 10	+5.7
E_{rH}/kJ mol^{-1}	15.0 ± 0.5	16.1	23.1	—	—
τ_{rH}^{298}/ps	35 ± 5	40.3	28.3	—	30[e]
τ_v^{298}/ps	8 ± 1	3.3	3.9	—	3.3
Δ^2/10^{18} s^{-2}	160 ± 10	6.6	4.6	—	5.6
$A_O/\hbar$/10^6 rad s^{-1}	38.6[d]	38.6	38.6	43 ± 14	33.3

[a] Ref. 20. [b] Ref. 25. [c] Ref. 46. [d] Fixed during the fitting procedure. [e] r_1: relaxivity, k_{ex}^{298}: water exchange rate, $\Delta H^{\ddagger}$: activation enthalpy for water exchange, $\Delta S^{\ddagger}$: activation entropy for water exchange, E_{rH}: activation energy for the rotational motion of the complex, τ_{RH}: rotational correlation time of the Mn^{2+}–H$_{water}$ vector, τ_v^{298}: correlation time for the modulation of zero-field splitting (ZFS), Δ^2: trace of the square of the transient ZFS tensor, $A_O/\hbar$: scalar coupling constant.

Table 7 Comparison of the relevant physicochemical data of the Mn(II) complexes formed with **L1** and other selected ligands

	[Mn(**L1**)(H$_2$O)]$^+$	[Mn(3,9-PC2A)(H$_2$O)][a]	[Mn(3,6-PC2A)(H$_2$O)][a]	[Mn(PC1A)(H$_2$O)]$^+$ [b]	[Mn(PC1P)(H$_2$O)][b]	[Mn(3,9-OPC2A)(H$_2$O)][c]	[Mn(PC2A-EA)(H$_2$O)][d]	[Mn(PC2A-BP)(H$_2$O)][e]
CN/q	7/1	7/1	7/1	6/1	6/1	7/1	7/0 7/1[f]	7/1
r_{1p}^{298g}	2.45	2.91	2.72	2.39	2.84	3.09	2.1[h]/3.5[i]	4.96/35.7[j]
$k_{ex}^{298}/10^7$ s^{-1}	0.45 ± 0.02	12.5 ± 1.2	14 ± 2.5	303 ± 19	177 ± 9	5.3 ± 0.4	4.0 ± 0.2	6.3 ± 0.2
$\Delta H^{\ddagger}$/kJ mol^{-1}	28.1 ± 2.1	37.5 ± 2.4	38.2 ± 3.9	13.0 ± 1.6	14.0 ± 1.2	28.5 ± 1.7	—	35.7 ± 0.1
$A_O/\hbar/10^6$ rad s^{-1}	38.6[k]	−42.4 ± 1.9	−44.6 ± 1.8	36.6 ± 1.3	39.9 ± 1.7	—	—	40.0

[a] Ref. 17. [b] Ref. 28. [c] Ref. 18. [d] Ref. 26. [e] Ref. 27. [f] Ref. 26 at pH values above 8.0. [g] Determined at 298 K and 0.49 T. [h] Determined at pH 6.0. [i] Determined at pH 8.4. [j] Ref. 53 measured in the presence of HSA. [k] Fixed during the fitting procedure.

remarkably low (<5 mM^{-1} s^{-1}) as compared to those for the parent Mn(15-pyN$_3$O$_2$) (~11.8 mM^{-1} s^{-1}), even considering the lower hydration number of **MnL1**. These differences indicate faster electron spin relaxation of **MnL1** reflected in higher values of τ_v^{298} and Δ^2 which might be related to the different symmetry of the two complexes; nevertheless any deeper interpretation is difficult, although some recent efforts have been made to relate the structure and the electron spin relaxation of Mn(II) complexes.[52] Finally, the rotational correlation time, τ_{RH}^{298} and the activation energy for the rotational motion of the complex, E_{rH}, as determined from the relaxivities, are similar to other data reported for complexes of similar size.

Conclusions

In the family of 15-membered pyridine-based macrocycles, we have prepared in a high yield a novel ligand, **L1**, which bears one acetate pendant arm in addition to macrocycle N and O donors in order to reinforce metal coordination. Its Mn(II) complex was characterized in the general context of MRI contrast agent development. pH-potentiometric studies evidence that the coordinating acetate function leads to higher thermodynamic stability for Mn(II), Zn(II), Cu(II) and Ca(II) complexes, in comparison with the parent 15-pyN$_3$O$_2$ macrocycle. The Mn(II) complex is fully formed at pH 7, as also confirmed by pH-dependent ^{1}H-relaxometry data. Despite the slower dissociation of **MnL1** with respect to Mn(15-pyN$_3$O$_2$), the kinetic inertness remains very modest.

While the addition of the acetate function on the macrocycle is beneficial for complex stability and resistance to dissociation, it has negative consequences in reducing the hydration number, and thus the relaxivity of **MnL1**. r_1 values are comparable to those of typical small Mn(II) chelates with q = 1, but about 40% lower than for bishydrated Mn(II) complexes such as Mn(15-pyN$_3$O$_2$). The water exchange rate is among the lowest ever measured for a Mn(II) complex, but it does not have a limiting effect on relaxivity.

Overall, these results indicate that **MnL1** is not suitable for *in vivo* applications, but they provide a better insight into the relationships between the structure of pyridine-based macrocyclic ligands and the MRI activity of their Mn(II) chelates.

Conflicts of interest

There are no conflicts to declare.

Acknowledgements

The authors gratefully acknowledge the financial support from the Palacký University Olomouc projects IGA_PrF_2021_009, IGA_PrF_2022_006, Palacký Endowement fund scholarship 2020 and 2022. The authors also thank Dr I. Nemec for the measurement of X-ray data and their analysis, and Dr A. Pallier for helping with ^{1}H NMRD profile measurements.

Notes and references

1 P. C. Lauterbur, *Nature*, 1973, **242**, 190–191.
2 P. Mansfield and P. Grannell, *Phys. Rev. B: Solid State*, 1975, **12**, 3618–3634.
3 R. Damadian, L. Minkoff, M. Goldsmith, M. Standford and J. Koutcher, *Science*, 1976, **194**, 1430–1432.
4 A. Merbach, E. Tóth and L. Helm, *The Chemistry of Contrast Agents in Medical Magnetic Resonance Imaging*, Wiley, 2013.
5 T. Grobner, *Nephrol., Dial., Transplant.*, 2006, **21**, 1104–1108.
6 R. Agarwal, S. M. Brunelli, K. Williams, M. D. Mitchell, H. I. Feldman and C. A. Umscheid, *Nephrol., Dial., Transplant.*, 2008, **24**, 856.
7 E. Di Gregorio, G. Ferruato, C. Furlan, S. Lanzardo, R. Nuzzi, E. Gianolio and S. Aime, *Invest. Radiol.*, 2018, **53**, 167–172.
8 E. Kanal and M. F. Tweedle, *Radiology*, 2015, **275**, 630–634.
9 ClinicalTrials.gov., **https://clinicaltrials.gov/ct2/show/NCT05413668**, date of access: 16 February 2023.
10 B. Drahos, I. Lukes and E. Toth, *Eur. J. Inorg. Chem.*, 2012, 1975–1986.
11 A. Gupta, P. Caravan, W. S. Price, C. Platas-Iglesias and E. M. Gale, *Inorg. Chem.*, 2020, **59**, 6648–6678.
12 M. Botta, F. Carniato, D. Esteban-Gómez, C. Platas-Iglesias and L. Tei, *Future Med. Chem.*, 2019, **11**, 1461–1483.
13 T. Inoue, T. Majid and R. G. Pautler, *Rev. Neurosci.*, 2011, **22**, 675–694.

14 S. Rivera-Mancía, C. Rios and S. Montes, *BioMetals*, 2011, **24**, 811–825.
15 Z. Garda, A. Forgacs, Q. N. Do, F. K. Kalman, S. Timari, Z. Baranyai, L. Tei, I. Toth, Z. Kovacs and G. Tircso, *J. Inorg. Biochem.*, 2016, **163**, 206–213.
16 M. Kueny-Stotz, A. Garofalo and D. Felder-Flesh, *Eur. J. Inorg. Chem.*, 2012, 1987–2005.
17 Z. Garda, E. Molnar, N. Hamon, J. L. Barriada, D. Esteban-Gomez, B. Varadi, V. Nagy, K. Pota, F. K. Kalman, I. Toth, N. Lihi, C. Platas-Iglesias, E. Toth, R. Tripier and G. Tircso, *Inorg. Chem.*, 2021, **60**, 1133–1148.
18 T. Csupasz, D. Szucs, F. K. Kalman, O. Holloczki, A. Fekete, D. Szikra, E. Toth, I. Toth and G. Tircso, *Molecules*, 2022, **27**, 371.
19 (*a*) D. Ndiaye, M. Sy, A. Pallier, S. Meme, I. de Silva, S. Lacerda, A. M. Nonat, L. J. Charbonnière and E. Toth, *Angew. Chem., Int. Ed.*, 2020, **59**, 11958–11963; (*b*) P. Cieslik, P. Comba, B. Dittmar, D. Ndiaye, É. Tóth, G. Velmurugan and H. Wadepohl, *Angew. Chem., Int. Ed.*, 2022, **61**, e202115580; (*c*) D. Ndiaye, P. Cieslik, H. Wadepohl, A. Pallier, S. Même, P. Comba and É. Tóth, *J. Am. Chem. Soc.*, 2022, **144**, 22212–22220.
20 B. Drahos, J. Kotek, P. Hermann, I. Lukes and E. Toth, *Inorg. Chem.*, 2010, **49**, 3224–3238.
21 D. P. Riley, S. L. Henke, P. J. Lennon, R. H. Weiss, W. L. Neumann, W. J. Rivers, Jr., K. W. Aston, K. R. Sample, H. Rahman, C. S. Ling, J. J. Shieh, D. H. Busch and W. Szulbinski, *Inorg. Chem.*, 1996, **35**, 5213–5231.
22 A. Dees, A. Zahl, R. Puchta, N. J. R. van Eikema Hommes, F. W. Heinemann and I. Ivanovic-Burmazovic, *Inorg. Chem.*, 2007, **46**, 2459–2470.
23 M. F. Cabral and R. Delgado, *Helv. Chim. Acta*, 1994, **77**, 515–524.
24 J. E. Newton and S. C. Jackels, *J. Coord. Chem.*, 1988, **19**, 265–277.
25 K. Pota, E. Molnar, F. K. Kalman, D. M. Freire, G. Tircso and K. N. Green, *Inorg. Chem.*, 2020, **59**, 11366–11376.
26 R. Botar, E. Molnar, G. Trencsenyi, J. Kiss, F. K. Kálmán and G. Tircsó, *J. Am. Chem. Soc.*, 2020, **142**, 1662–1666.
27 F. K. Kalman, V. Nagy, B. Varadi, Z. Garda, E. Molnar, G. Trencsenyi, J. Kiss, S. Meme, W. Meme, E. Toth and G. Tircso, *J. Med. Chem.*, 2020, **63**, 6057–6065.
28 B. Drahos, J. Kotek, I. Cisarova, P. Hermann, L. Helm, I. Lukes and E. Toth, *Inorg. Chem.*, 2011, **50**, 12785–12801.
29 S. Anbu, S. H. L. Hoffmann, F. Carniato, L. Kennig, T. W. Price, T. J. Prior, M. Botta, A. F. Martins and G. J. Stasiuk, *Angew. Chem., Int. Ed.*, 2021, **60**(19), 10736–10744.
30 S. Laine, C. S. Bonnet, F. K. Kálmán, Z. Garda, A. Pallier, F. Caillé, F. Suzenet, G. Tircsó and É. Tóth, *New J. Chem.*, 2018, **42**, 8012.
31 A. Forgács, R. Pujales-Paradela, M. Regueiro-Figueroa, L. Valencia, D. Esteban-Gómez, M. Botta and C. Platas-Iglesias, *Dalton Trans.*, 2017, **46**, 1546.
32 E. M. Gale, I. P. Atanasova, F. Blasi, I. Ay and P. Caravan, *J. Am. Chem. Soc.*, 2015, **137**, 15548–15557.
33 P. Antal, B. Drahos, R. Herchel and Z. Travnicek, *Inorg. Chem.*, 2016, **55**, 5957–5972.
34 G. M. Sheldrick, *Acta Crystallogr., Sect. C: Struct. Chem.*, 2015, **71**, 3–8.
35 O. V. Dolomanov, L. J. Bourhis, R. J. Gildea, J. A. K. Howard and H. Puschmann, *J. Appl. Crystallogr.*, 2009, **42**, 339–341.
36 C. F. Macrae, I. J. Bruno, J. A. Chisholm, P. R. Edgington, P. McCabe, E. Pidcock, L. Rodriguez-Monge, R. Taylor, J. van de Streek and P. A. Wood, *J. Appl. Crystallogr.*, 2008, **41**, 466–470.
37 A. E. Martell and R. J. Motekaitis, *Determination and use of stability constants*, VCH Publishers, 1992.
38 P. Gans, A. Sabatini and A. Vacca, *Talanta*, 1996, **43**, 1739–1753.
39 D. S. Raiford, C. L. Fisk and E. D. Becker, *Anal. Chem.*, 1979, **51**, 2050–2051.
40 E. Toth, L. Helm and A. Merbach, in *The Chemistry of Contrast Agents in Medical Magnetic resonance Imaging*, ed. A. Merbach, L. Helm and E. Toth, John Wiley & Sons, Chichester, 2nd edn, 2013, pp. 25–81.
41 I. Meunier, A. K. Mishra, B. Hanquet, P. Cocolios and R. Guilard, *Can. J. Chem.*, 1995, **73**, 685–695.
42 R. Uzal-Varela, F. Pérez-Fernández, L. Valencia, A. Rodríguez-Rodríguez, C. Platas-Iglesias, P. Caravan and D. Esteban-Gómez, *Inorg. Chem.*, 2022, **61**, 14173–14186.
43 W. D. Kim, D. C. Hrncir, G. E. Kiefer and A. D. Sherry, *Inorg. Chem.*, 1995, **34**, 2225–2232.
44 D. Esteban-Gomez, C. Cassino, M. Botta and C. Platas-Iglesias, *RSC Adv.*, 2014, **4**, 7094–7103.
45 B. Drahoš, V. Kubíček, C. S. Bonnet, P. Hermann, I. Lukeš and E. Tóth, *Dalton Trans.*, 2011, **40**, 1945–1951.
46 Y. Ducommun, K. E. Newmann and A. E. Merbach, *Inorg. Chem.*, 1980, **19**, 3696–3703.
47 J. Maigut, R. Meier, A. Zahl and R. van Eldik, *Inorg. Chem.*, 2008, **47**, 5702–5719.
48 S. H. Koenig, C. Baglin, R. D. Brown III and C. F. Brewer, *Magn. Reson. Med.*, 1984, **1**, 496–501.
49 I. Bertini, F. Briganti, Z. Xia and C. Luchinat, *J. Magn. Reson., Ser. A*, 1993, **101**, 198–201.
50 E. M. Gale, J. Zhu and P. Caravan, *J. Am. Chem. Soc.*, 2013, **135**, 18600.
51 J. A. Peters and C. F. G. C. Geraldes, *Inorganics*, 2018, **6**(4), 116.
52 R. Uzal-Varela, L. Valencia, D. Lalli, M. Maneiro, D. Esteban-Gómez, C. Platas-Iglesias, M. Botta and A. Rodríguez-Rodríguez, *Inorg. Chem.*, 2021, **60**, 15055–15068.
53 G. Rolla, V. de Biasio, G. B. Giovenzana, M. Botta and L. Tei, *Dalton Trans.*, 2018, **47**, 10660–10670.